J. Fluid Mech. (2017), *vol.* 822, *pp.* 170–185.
doi:10.1017/jfm.2017.275

Linear stability of a viscoelastic liquid flow on an oscillating plane

Arghya Samanta†

Department of Applied Mechanics, Indian Institute of Technology Delhi, Hauz Khas, New Delhi 110016, India

(Received 11 November 2016; revised 11 March 2017; accepted 22 April 2017; first published online 31 May 2017)

Linear stability of a viscoelastic liquid on an oscillating plane is studied for disturbances of arbitrary wavenumbers. The main aim is to extend the earlier study of Dandapat & Gupta (*J. Fluid Mech.*, vol. 72, 1975, pp. 425–432) to the finite wavenumber regime, which has not been attempted so far in the literature. The Orr–Sommerfeld boundary value problem is formulated for an unsteady base flow, and it is resolved numerically based on the Chebyshev spectral collocation method along with the Floquet theory. The analytical solution predicts that U-shaped unstable regions appear in the separated bandwidths of the imposed frequency, and the dominant mode of the long-wave instability intensifies in the presence of the viscoelastic parameter. The numerical solution shows that oblique neutral curves come out from the branch points of the U-shaped neutral curves at finite wavenumber and continue with the imposed frequency until the curves cross the next U-shaped neutral curve. As a consequence, in the finite wavenumber regime, no stable bandwidth of the imposed frequency is predicted by the long-wavelength analysis. Further, in some frequency ranges, the finite wavenumber instability is more dangerous than the long-wave instability.

Key words: non-Newtonian flows, parametric instability, viscoelasticity

1. Introduction

During the last few decades, studies of viscoelastic liquid flow have been of special interest in the chemical industry due to its drag reduction property (Savins 1967). Further, such liquids are common in coating technology due to their different mechanical properties (Dávalos-Orozco 2013). On the other hand, the instabilities of a viscoelastic liquid occur in a wide variety of applications including lubrication, coating and various types of polymer processing operations (Larson 1992; Shaqfeh 1996). In this context, Dandapat & Gupta (1975) first initiated the present model as an extension of the unsteady Newtonian flow on an oscillatory plane (Yih 1968) to understand the dynamic behaviour of viscoelasticity when the base flow is unsteady. In particular, the unsteady base flow makes the problem troublesome to deal with even numerically. Besides, the present model is relevant in physiological applications for understanding the viscoelastic blood flow through vessels and arterial stenosis in

† Email address for correspondence: arghyar@gmail.com

detail, which may lead to early detection and prevention of cardiovascular diseases (Grotberg & Jensen 2004; Ikbal 2012). These facts have motivated us to explore the present problem.

The study of the Newtonian liquid flow on a horizontal oscillating plane was pioneered by Yih (1968) to take into account the effect of unsteady base flow on the long-wave modes. The regular perturbation method based on the Floquet theory was used to resolve the time-dependent Orr–Sommerfeld boundary value problem. As discussed by Yih (1968), the long-wave mode can be unstable at a sufficiently large amplitude of oscillation. Later, the same problem was tackled by Or (1997) to decipher the finite wavelength instability for infinitesimal disturbances with arbitrary wavenumbers. It was shown that long-wavelength unstable regions appear in the separated bandwidths of the imposed frequency, and the finite wavelength instability appears through the branch points of the long-wave neutral curves. Moreover, Or (1997) showed that the finite wavenumber mode is more unstable than the long-wave mode in a few regimes of the imposed frequency. Recently, Yih's model was extended by Gao & Lu (2006, 2008) to investigate the effect of insoluble surfactants on the long-wave modes and the finite wavenumber modes. As reported by Gao & Lu (2006, 2008), the long-wave mode can be stabilized by using an insoluble surface surfactant. Owing to the destabilizing property of an electric field on the long-wave mode, the joint effect of an insoluble surfactant and an electric field on the long-wave instability for an oscillatory flow was investigated by Samanta (2009). It was shown the growth rate of the long-wave mode increases in the presence of an electric field but decreases with the presence of an insoluble surfactant. Unlike a horizontal oscillation of a plane, the instability of a Newtonian liquid layer flowing down a vibrating inclined plane was studied by Woods & Lin (1995), Lin, Chen & Woods (1996) and Burya & Shkadov (2001). In fact, in that model, the horizontal plane performs an oscillatory motion perpendicular to its own plane, and the resulting acceleration has two components in the streamwise flow and cross-streamwise flow directions. As a consequence, Faraday waves develop on the surface due to an effective modulation of gravity. Both subharmonic and synchronous solutions occur. However, in the present model, no subharmonic solution exists.

Motivated by Yih's work (Yih 1968), the model of unsteady Newtonian flow was extended to the model of unsteady non-Newtonian viscoelastic flow by Dandapat & Gupta (1975) to perform linear stability analysis in the long-wave regime. As reported by these authors, the viscoelastic parameter exhibits a destabilizing effect on the long-wave mode. However, in some frequency ranges, the viscoelastic parameter exhibits a stabilizing effect on the long-wave mode. However, so far no attempt has been made to decipher the finite wavenumber linear stability analysis corresponding to viscoelastic liquid.

In this article, the main purpose is to fill the gap that remained in the previous study (Dandapat & Gupta 1975), i.e. to explore infinitesimal disturbances with arbitrary wavenumbers on the surface of a viscoelastic liquid on an oscillating plane. It is observed that a long-wave unstable region appears in the separated bandwidths of the imposed frequency. Outside of these frequency bandwidths, the long-wave disturbances are stable. In fact, the stabilizing effect of viscoelasticity on the long-wave mode was found by Dandapat & Gupta (1975) in these stable frequency bandwidths. However, in the finite wavenumber regime, no stable frequency bandwidth exists, because finite wavenumber modes appear in these stable frequency bandwidths, as predicted by the long-wavelength analysis. In the presence of the viscoelastic parameter, the most unstable mode becomes stronger than that of Newtonian liquid.

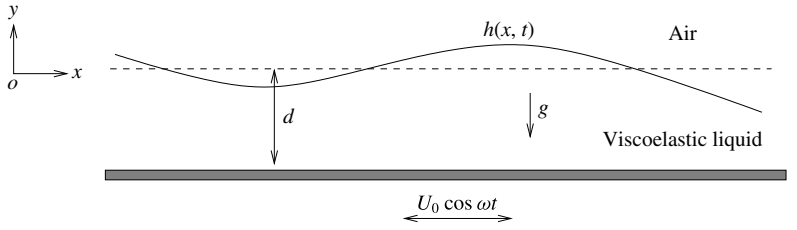

FIGURE 1. Schematic diagram of a viscoelastic liquid on an oscillating plane.

2. Mathematical formulation

Consider an incompressible two-dimensional viscoelastic liquid film flow with density ρ, limiting viscosity μ and surface tension σ on a horizontal plane, where the motion of the viscoelastic liquid starts due to an oscillation of the plane in the horizontal direction with a velocity $\hat{\boldsymbol{i}} U_0 \cos \omega t$, where $\hat{\boldsymbol{i}}$ is a unit vector in the streamwise direction. Figure 1 shows a schematic diagram of the present model, where the origin is located at the free surface, and the x and y axes are directed along the streamwise flow and the cross-streamwise flow respectively. Walter's liquid B'', which is an approximation to the first order in elasticity from the Newtonian behaviour and possesses a short or rapidly fading memory, is considered in the current study. The liquid B'' satisfies the following constitutive equation of state (Beard & Walters 1964; Andersson & Dahl 1999):

$$\tau_{ij} = -p\delta_{ij} + \tau'_{ij}, \tag{2.1}$$

where τ_{ij} is the stress tensor, δ_{ij} is the Kronecker delta, p is the pressure and τ'_{ij} is defined by

$$\tau'_{ij} = 2\mu e_{ij} - 2M_0 \frac{\delta}{\delta t} e_{ij}, \tag{2.2}$$

where $2\mu e_{ij}$ is the Newtonian viscous stress contribution, $2M_0(\delta/\delta t)e_{ij}$ is the elastic stress contribution, M_0 is the viscoelastic coefficient, $e_{ij} = (\partial_i u_j + \partial_j u_i)/2$ is the strain rate tensor and the co-rotational derivative of the strain rate tensor e_{ij} is defined by

$$\frac{\delta}{\delta t} e_{ij} = \partial_t e_{ij} + u_k \partial_k e_{ij} - \partial_k u_j e_{ik} - \partial_k u_i e_{kj}. \tag{2.3}$$

Obviously, the constitutive equation (2.1) recovers the Newtonian behaviour when the viscoelastic coefficient M_0 is set to zero. The general form of the constitutive equation can be found in Oldroyd (1950), Beard & Walters (1964), Bird *et al.* (1987) and Barnes, Hutton & Walters (1989). The rheological model given in the constitutive equation (2.1) is obtained by removing the relaxation time parameter, and the reduced model is referred to as Walter's liquid B'' (Beard & Walters 1964; Andersson & Dahl 1999). A mixture of polymethyl methacrylate in pyridine with density $\rho = 0.98 \times 10^3$ kg m^{-3}, limiting viscosity $\mu = 0.79$ N s m^{-2} and viscoelastic coefficient $M_0 = 0.04$ N s^2 m^{-2} is an example of Walter's liquid B'' (Walters 1960; Andersson & Dahl 1999).

The mass and momentum conservation equations that govern the flow are

$$\partial_i u_i = 0, \tag{2.4}$$

$$\rho(\partial_t u_i + u_j \partial_j u_i) = \rho g_i + \partial_j \tau_{ij}, \tag{2.5}$$

where $g_x = 0$ and $g_y = -g$, g is the gravitational acceleration. The associated boundary conditions are as follows. (i) At the plane $y = -d$,

$$u_x = u = U_0 \cos \omega t, \qquad u_y = v = 0. \tag{2.6a,b}$$

(ii) At the free surface $y = h(x, t)$, the balances of tangential and normal stresses,

$$\tau_{ij} n_j t_i = 0, \quad \tau_{ij} n_i n_j = \sigma \partial_{xx} h / [1 + (\partial_x h)^2]^{3/2}, \tag{2.7a,b}$$

where $\boldsymbol{n} = (n_x \hat{\boldsymbol{i}} + n_y \hat{\boldsymbol{j}})$ is the unit normal vector, $\boldsymbol{t} = (t_x \hat{\boldsymbol{i}} + t_y \hat{\boldsymbol{j}})$ is the unit tangent vector and $\hat{\boldsymbol{j}}$ is a unit vector in the cross-streamwise direction. (iii) The kinematic boundary condition at the free surface $y = h(x, t)$ is given by

$$\partial_t f + u_i \partial_i f = 0, \tag{2.8}$$

where $f(x, t) = h(x, t) - y$. Since the present study is an unsteady flow problem and the primary flow occurs due to the horizontal oscillation of the plane, an appropriate scale for time is the inverse of imposed frequency. Next, the velocity scale is obtained from the balance of the inertia term and the viscous friction term. Accordingly, the governing equations (2.4)–(2.8) are normalized by choosing d as the length scale, ν/d as the velocity scale, $1/\omega$ as the time scale and $\rho\nu^2/d^2$ as the pressure scale. The proposed characteristic scales lead to a set of dimensionless parameters: the Reynolds number, $Re = U_0 d/\nu$, shows the effect of the oscillation amplitude, the Galileo number, $\chi = gd^3/(2\nu^2)$, shows the effect of gravity, the capillary number, $\zeta = \rho\nu^2/(\sigma d) = \mu(\nu/d)/\sigma$, shows the effect of surface tension, the viscoelastic parameter, $M = M_0/(\rho d^2)$, shows the effect of viscoelasticity and the Womersley number, $\beta = \sqrt{\omega d^2/(2\nu)}$, shows the effect of the imposed frequency. The dimensionless viscoelastic parameter M compares the square of the elastic length M_0/ρ with the square of the mean film thickness d^2, while the dimensionless imposed frequency $2\beta^2$ compares the square of the mean film thickness d^2 with the square of the Stokes layer thickness ν/ω, or, equivalently, it compares the viscous time scale d^2/ν with the frequency time scale $1/\omega$.

Consider a unidirectional time periodic parallel flow with constant film thickness. Consequently, the governing equations (2.4)–(2.8) are simplified to the following dimensionless form:

$$2\beta^2 \partial_t U_x = -\partial_x P + \partial_{yy} U_x - 2\beta^2 M \partial_{yyt} U_x, \quad \partial_y P + 2\chi = 0, \tag{2.9a,b}$$

$$U_x = Re \cos t, \quad \text{at } y = -1, \quad \partial_y U_x - 2\beta^2 M \partial_{yt} U_x = 0, \quad P = 0, \quad \text{at } y = 0. \tag{2.10a,b}$$

The base flow solution can be expressed as

$$U_x = U(y, t) = \mathrm{Re}\left[\frac{Re \cosh[\Omega(1 + \mathrm{i}S)y]\mathrm{e}^{\mathrm{i}t}}{\cosh[\Omega(1 + \mathrm{i}S)]}\right], \quad U_y = V(y, t) = 0, \quad P(y) = -2\chi y, \tag{2.11a–c}$$

where $S = [(1 + 4M^2\beta^4)^{1/2} + 2M\beta^2]$ and $\Omega = \beta[\{(1 + 4M^2\beta^4)^{1/2} - 2M\beta^2\}/(1 + 4M^2\beta^4)]^{1/2}$. Here, Re$[\cdots]$ represents the real part of that complex function. It should be noted that the base flow is strongly dependent on the viscoelastic parameter M. In the absence of the viscoelastic parameter ($M = 0$), the base flow velocity is identical to that of Or (1997). Moreover, the base velocity coincides with that of Dandapat & Gupta (1975) when the characteristic scales are the same.

3. Orr–Sommerfeld boundary value problem

The primary instability is studied by considering a two-dimensional infinitesimal disturbance $q = Q + \tilde{q}$ on the base flow, where q represents the flow variables, Q represents the basic quantities and $\tilde{q}$ represents the perturbation quantities. By substituting q in the dimensionless form of the governing equations (2.4)–(2.8) and linearizing with respect to the base state, we obtain the following linearized perturbation equations:

$$\partial_x \tilde{u} + \partial_y \tilde{v} = 0, \tag{3.1}$$

$$\begin{aligned} 2\beta^2 \partial_t \tilde{u} + (U\partial_x \tilde{u} + \tilde{v}\partial_y U) = -\partial_x \tilde{p} + (\partial_{xx}\tilde{u} + \partial_{yy}\tilde{u}) - 2\beta^2 M(\partial_{xxt}\tilde{u} + \partial_{yyt}\tilde{u}) \\ - M[U(\partial_{xxx}\tilde{u} + \partial_{xyy}\tilde{u}) - \partial_y U(\partial_{xy}\tilde{u} + \partial_{xx}\tilde{v}) + \tilde{v}\partial_{yyy}U - \partial_y \tilde{v}\partial_{yy}U], \end{aligned} \tag{3.2}$$

$$\begin{aligned} 2\beta^2 \partial_t \tilde{v} + U\partial_x \tilde{v} = -\partial_y \tilde{p} + (\partial_{xx}\tilde{v} + \partial_{yy}\tilde{v}) - 2\beta^2 M(\partial_{xxt}\tilde{v} + \partial_{yyt}\tilde{v}) \\ - M[U(\partial_{xxx}\tilde{v} + \partial_{xyy}\tilde{v}) - 2\partial_y U\partial_{xy}\tilde{v} - \partial_{yy}U\partial_x \tilde{v}], \end{aligned} \tag{3.3}$$

$$\tilde{u} = 0, \quad \tilde{v} = 0, \quad \text{at } y = -1, \tag{3.4}$$

$$\begin{aligned} \partial_y \tilde{u} + \partial_x \tilde{v} + \tilde{h}\partial_{yy}U - 2\beta^2 M(\partial_{yt}\tilde{u} + \partial_{xt}\tilde{v} + \tilde{h}\partial_{yyt}U) \\ - M[U(\partial_{xx}\tilde{v} + \partial_{xy}\tilde{u}) + \tilde{v}\partial_{yy}U] = 0, \quad \text{at } y = 0, \end{aligned} \tag{3.5}$$

$$-\tilde{p} + 2\chi\tilde{h} + 2\partial_y \tilde{v} - 4\beta^2 M\partial_{ty}\tilde{v} - 2MU\partial_{xy}\tilde{v} = (1/\zeta)\partial_{xx}\tilde{h}, \quad \text{at } y = 0, \tag{3.6}$$

$$2\beta^2 \partial_t \tilde{h} + U\partial_x \tilde{h} = \tilde{v}, \quad \text{at } y = 0. \tag{3.7}$$

Now, the stream function $\tilde{\psi}$ is introduced by using the relations $\tilde{u} = \partial_y \tilde{\psi}$ and $\tilde{v} = -\partial_x \tilde{\psi}$. Next, the solution of the perturbation equations (3.1)–(3.7) is assumed in the normal mode form $\tilde{\psi}(x, y, t) = \phi(y, t)\exp(\mathrm{i}kx)$ and $\tilde{h}(x, t) = \eta(t)\exp(\mathrm{i}kx)$, where ϕ and η are respectively the amplitude of the perturbation stream function and the deformed free surface. Here, k is the wavenumber. By inserting $\tilde{\psi}$ and $\tilde{h}$ into the perturbation equations (3.1)–(3.7) and eliminating the pressure term from the momentum equations, we obtain the following time-dependent Orr–Sommerfeld boundary value problem (OS BVP) for a viscoelastic liquid:

$$2\beta^2(\mathcal{L} + M\mathcal{L}^2)\partial_t \phi = \mathcal{L}^2\phi - \mathrm{i}k[U(\mathcal{L} + M\mathcal{L}^2) - (\mathcal{D}^2 U + M\mathcal{D}^4 U)]\phi, \tag{3.8}$$

$$\phi = \mathcal{D}\phi = 0, \quad \text{at } y = -1, \tag{3.9}$$

$$\begin{aligned} 2\beta^2 M(\mathcal{L} + 2k^2)\partial_t \phi = (\mathcal{L} + 2k^2)\phi - Mik[U(\mathcal{L} + 2k^2) - \mathcal{D}^2 U]\phi \\ + [\mathcal{D}^2 U - 2\beta^2 M\mathcal{D}^2 \partial_t U]\eta, \quad \text{at } y = 0, \end{aligned} \tag{3.10}$$

$$\begin{aligned} 2\beta^2[\mathcal{D} + M(\mathcal{L} - 2k^2)\mathcal{D}]\partial_t \phi = (\mathcal{L} - 2k^2)\mathcal{D}\phi - 2\mathrm{i}k\left(\chi + \frac{k^2}{2\zeta}\right)\eta \\ - \mathrm{i}k[U\{\mathcal{D} + M(\mathcal{L} - 2k^2)\mathcal{D}\} + M(\mathcal{D}^2 U\mathcal{D} - \mathcal{D}^3 U)]\phi, \quad \text{at } y = 0, \end{aligned} \tag{3.11}$$

$$2\beta^2 \partial_t \eta = -\mathrm{i}k\phi - \mathrm{i}kU\eta, \quad \text{at } y = 0, \tag{3.12}$$

where $\mathcal{D} = \partial_y$ and $\mathcal{L} = \partial_{yy} - k^2$ are differential operators. When the viscoelastic parameter M vanishes, the present OS BVP (3.8)–(3.12) reduces to the time-dependent OS BVP for a Newtonian liquid (Or 1997). The difference in the coefficients from the OS BVP obtained by Dandapat & Gupta (1975) is attributed to the choice of various characteristic scales.

4. Long-wavelength expansion

The time-dependent OS BVP (3.8)–(3.12) with periodic coefficients is resolved based on the long-wavelength expansion ($k \to 0$) along with the Floquet theory proposed by Yih (1968). Consequently, the solution is assumed in the following form:

$$\begin{bmatrix} \phi(y,t) \\ \eta(t) \end{bmatrix} = \mathrm{e}^{\delta t} \begin{bmatrix} \phi_0(y,t) + k\phi_1(y,t) + \cdots \\ \eta_0(t) + k\eta_1(t) + \cdots \end{bmatrix}, \tag{4.1}$$

where the Floquet exponent δ is of the form

$$\delta = \delta_0 + k\delta_1 + k^2\delta_2 + \cdots . \tag{4.2}$$

To take into account the effect of surface tension in the first-order formulation, we consider the capillary number $\zeta \sim O(k^2)$. By inserting (4.1) and (4.2) into the OS BVP (3.8)–(3.12) and collecting the leading-order $O(k^0)$ terms, we obtain the following set of equations:

$$2\beta^2(\mathcal{D}^2 + M\mathcal{D}^4)(\partial_t\phi_0 + \delta_0\phi_0) = \mathcal{D}^4\phi_0, \tag{4.3}$$

$$\phi_0 = \mathcal{D}\phi_0 = 0, \quad \text{at } y = -1, \tag{4.4}$$

$$2\beta^2 M\mathcal{D}^2(\partial_t\phi_0 + \delta_0\phi_0) = \mathcal{D}^2\phi_0 + (\mathcal{D}^2U - 2\beta^2 M\mathcal{D}^2\partial_t U)\eta_0, \quad \text{at } y = 0, \tag{4.5}$$

$$2\beta^2(\mathcal{D} + M\mathcal{D}^3)(\partial_t\phi_0 + \delta_0\phi_0) = \mathcal{D}^3\phi_0, \quad \text{at } y = 0, \tag{4.6}$$

$$2\beta^2(\partial_t\eta_0 + \delta_0\eta_0) = 0, \quad \text{at } y = 0. \tag{4.7}$$

Since $\eta_0(t)$ is a periodic function of t, the kinematic boundary condition (4.7) leads to an admissible solution $\delta_0 = 0$. Without loss of generality, we choose $\eta_0 = 1$. Otherwise, $\delta_0 \neq 0$ supplies a damped Floquet mode demonstrated by Yih (1968), and that damped mode is not of interest here. By substituting the values of δ_0 and η_0 and solving (4.3)–(4.6), the leading-order solution can be expressed as

$$\phi_0(y,t) = \mathrm{Re}\left[Re \frac{\{1 - \cosh[\Omega(1 + \mathrm{i}S)(y+1)]\}\mathrm{e}^{\mathrm{i}t}}{\cosh^2[\Omega(1 + \mathrm{i}S)]} \right]. \tag{4.8}$$

Obviously, ϕ_0 relies on the viscoelastic parameter M. In the limit $M \to 0$, the reduced solution (4.8) is identical to that of Yih (1968) when the characteristic scales are the same. For the first-order $O(k)$ approximation, we have the following set of equations:

$$\begin{aligned} 2\beta^2(\mathcal{D}^2 + M\mathcal{D}^4)(\partial_t\phi_1 + \delta_1\phi_0 + \delta_0\phi_1) = \mathcal{D}^4\phi_1 - \mathrm{i}\,[\, U(\mathcal{D}^2 + M\mathcal{D}^4) \\ - (\mathcal{D}^2U + M\mathcal{D}^4U)\,]\,\phi_0, \end{aligned} \tag{4.9}$$

$$\phi_1 = \mathcal{D}\phi_1 = 0, \quad \text{at } y = -1, \tag{4.10}$$

$$\begin{aligned} 2\beta^2 M\mathcal{D}^2(\partial_t\phi_1 + \delta_1\phi_0 + \delta_0\phi_1) = \mathcal{D}^2\phi_1 - M\mathrm{i}(U\mathcal{D}^2 - \mathcal{D}^2U)\phi_0 \\ + (\mathcal{D}^2U - 2\beta^2 M\mathcal{D}^2\partial_t U)\eta_1, \quad \text{at } y = 0, \end{aligned} \tag{4.11}$$

$$\begin{aligned} 2\beta^2(\mathcal{D} + M\mathcal{D}^3)(\partial_t\phi_1 + \delta_1\phi_0 + \delta_0\phi_1) = \mathcal{D}^3\phi_1 - 2\mathrm{i}\left(\chi + \frac{k^2}{2\zeta}\right)\eta_0 \\ - \mathrm{i}[U(\mathcal{D} + M\mathcal{D}^3) + M(\mathcal{D}^2U\mathcal{D} - \mathcal{D}^3U)]\phi_0, \quad \text{at } y = 0, \end{aligned} \tag{4.12}$$

$$2\beta^2(\partial_t\eta_1 + \delta_1\eta_0 + \delta_0\eta_1) = -\mathrm{i}\phi_0 - \mathrm{i}U\eta_0, \quad \text{at } y = 0. \tag{4.13}$$

Since $\phi_0(y,t)$, $U(y,t)$ and $\eta_0(t)$ are all periodic functions of time, to obtain a periodic solution $\eta_1(t)$ from the kinematic boundary condition (4.13), we must have $\delta_1 = 0$. As a result, (4.13) reduces to the following form:

$$2\beta^2\partial_t\eta_1 = -\mathrm{i}(\phi_0 + U), \tag{4.14}$$

which yields a periodic solution

$$\eta_1(t) = -\frac{\mathrm{i}Re}{2\beta^2}\mathrm{Im}\left[\frac{\mathrm{e}^{\mathrm{i}t}}{\cosh^2[\Omega(1+\mathrm{i}S)]}\right], \tag{4.15}$$

where $\mathrm{Im}[\cdots]$ represents the imaginary part of that complex function. Indeed, the first-order equations (4.9)–(4.12) possess steady and unsteady terms. As the Floquet exponent is independent of time, the solution of only first-order steady equations is sufficient to compute the next-order Floquet exponent δ_2. Therefore, we shall focus solely on the steady equations in the subsequent calculations. After some mathematical manipulation, the solution of the first-order steady equations can be expressed as

$$\phi_1^{\mathcal{S}}(y) = a_1 + b_1 y + c_1 y^2 + d_1 y^3 - 2\mathrm{i}\,Re^2\mathrm{Re}[I_0] + 2\mathrm{i}\,Re^2\mathrm{Re}[I_1], \tag{4.16}$$

where superscript '$\mathcal{S}$' denotes the steady solution and

$$I_0 = \frac{\mathrm{i}A^2(1+\gamma^2)(1-4M^2\beta^4)}{8\beta^2 S^2}\tanh[\Omega(1+\mathrm{i}S)]\{S^4\sinh(2\Omega y) + \mathrm{i}\sin(2\Omega S y)\}, \tag{4.17}$$

$$I_1 = \frac{\mathrm{i}A^2(1+\gamma^2)}{2\beta^2}\frac{\cosh[\Omega(1+\mathrm{i}S)y]}{\cosh[\Omega(1-\mathrm{i}S)]}, \tag{4.18}$$

$$\left.\begin{aligned} A = \frac{\cos(\Omega S)\cosh\Omega}{2[\cos^2(\Omega S) + \sinh^2\Omega]}, \quad \gamma = \tan(\Omega S)\tanh\Omega, \\ d_1 = \mathrm{i}[\chi/3 + k^2/(6\zeta)], \quad c_1 = 0, \end{aligned}\right\} \tag{4.19}$$

$$b_1 = -3d_1 + \frac{\mathrm{i}\,Re^2A^2(1+\gamma^2)}{\beta^2}R_2, \quad a_1 = -2d_1 + \frac{\mathrm{i}\,Re^2A^2(1+\gamma^2)}{\beta^2}(R_2 - R_1), \tag{4.20a,b}$$

where R_1 and R_2 are of the form

$$R_1 = \mathrm{Re}\left[\frac{\mathrm{i}}{4S^2}\tanh[\Omega(1+\mathrm{i}S)][S^4\sinh 2\Omega + \mathrm{i}\sin(2\Omega S)](1-4M^2\beta^4) + \mathrm{i}\frac{\cosh[\Omega(1+\mathrm{i}S)]}{\cosh[\Omega(1-\mathrm{i}S)]}\right], \tag{4.21}$$

$$R_2 = \mathrm{Re}\left[\frac{\mathrm{i}\Omega}{2S}\tanh[\Omega(1+\mathrm{i}S)][S^3\cosh 2\Omega + \mathrm{i}\cos(2\Omega S)](1-4M^2\beta^4) - \frac{(1+S^2)\Omega\sinh[\Omega(1+\mathrm{i}S)]}{(S+\mathrm{i})\cosh[\Omega(1-\mathrm{i}S)]}\right]. \tag{4.22}$$

Now, in order to compute the Floquet exponent δ_2, we consider the second-order $O(k^2)$ approximation of the kinematic boundary condition at $y = 0$,

$$2\beta^2(\partial_t\eta_2 + \delta_2\eta_0 + \delta_1\eta_1 + \delta_0\eta_2) = -\mathrm{i}\phi_1 - \mathrm{i}U\eta_1. \tag{4.23}$$

Again, δ_2 is independent of time, so we must have

$$\delta_2 = -\frac{\mathrm{i}}{2\beta^2}[\phi_1^{\mathcal{S}} + (U\eta_1)^{\mathcal{S}}] = \frac{1}{2\beta^2}\left[2\mathrm{i}d_1 - \frac{Re^2A^2(1+\gamma^2)}{\beta^2}(R_1 - R_2)\right]. \tag{4.24}$$

Inserting the values of δ_0, δ_1 and δ_2, the Floquet exponent δ can be written as

$$\delta = k^2\delta_2 + O(k^3) = \frac{k^2}{2\beta^2}\left[2\mathrm{i}d_1 - \frac{A^2Re^2(1+\gamma^2)}{\beta^2}(R_1 - R_2)\right] + O(k^3)$$

$$= \frac{k^2}{2\beta^2}\left[\underbrace{\frac{A^2Re^2(1+\gamma^2)}{\beta^2}(R_2 - R_1)}_{VECT} - \underbrace{\frac{2\chi}{3}}_{GT} - \underbrace{\frac{k^2}{3\zeta}}_{ST}\right] + O(k^3), \tag{4.25}$$

where *VECT*, *GT* and *ST* represent the viscoelastic coupling term, gravity term and surface tension term respectively. Equation (4.25) demonstrates that the Floquet exponent δ is simply a combination of three terms *VECT*, *GT* and *ST*, and its magnitude will reduce in the presence of gravity and surface tension. In other words, gravity and surface tension exhibit a stabilizing effect on the long-wave mode.

We have noticed that the leading- and first-order solutions of the kinematic boundary condition (3.12) yield $\delta_0 = 0$ and $\delta_1 = 0$. Hence, in the long-wavelength limit $k \to 0$, the amplitude $[\propto \mathrm{e}^{\delta t} = \mathrm{e}^{k^2\delta_2 + O(k^3)}]$ of an infinitesimal disturbance will grow or decay exponentially with time if $\delta_2 >$ or < 0, or, equivalently, if the following criterion is satisfied:

$$\frac{2\chi}{Re^2} < \text{or} > \left[\frac{3A^2(1+\gamma^2)}{\beta^2}(R_2 - R_1) - \frac{k^2}{\zeta Re^2}\right] = L(\beta). \tag{4.26}$$

Therefore, one can conclude that the long-wavelength disturbance will be stable if $\delta_2 < 0$; otherwise, it will be unstable if $\delta_2 > 0$. In the absence of elasticity and for a low magnitude of surface tension, equation (4.26) coincides with that of Yih (1968) and Or (1997), where $2\chi/Re^2 = Fr^{-2} = gd/U_0^2$, and $L(\beta) = [3A^2(1+\gamma^2)/\beta^2](R_2 - R_1)$ in Yih's notation. In addition, the expression (4.26) is identical to that of Dandapat & Gupta (1975) when the characteristic scales are the same.

In order to analyse the effect of surface tension on the long-wave mode independently, a new parameter is introduced: $\zeta^* = k^2/\zeta$ represents the effect of surface tension. The neutral stability criterion $\delta_2 = 0$ leads to an analytical expression of the Reynolds number as a function of the dimensionless imposed frequency $2\beta^2$,

$$Re = \left[(2\chi + \zeta^*) \Big/ \left\{\frac{6A^2(1+\gamma^2)}{2\beta^2}(R_2 - R_1)\right\}\right]^{1/2}. \tag{4.27}$$

Figure 2(*a*) shows that U-shaped neutral curves appear in the separated bandwidths of the imposed frequency when $k \to 0$. Therefore, the long-wavelength instability prevails only in these frequency bandwidths. Outside of these bandwidths, all infinitesimal disturbances are stable. This result is completely consistent with that of Dandapat & Gupta (1975). For this reason, the stabilizing effect of the viscoelastic parameter was found by Dandapat & Gupta (1975) in these stable bandwidths of the imposed frequency. Moreover, in each unstable frequency bandwidth, there exists a critical Reynolds number ($Re = U_0 d/\nu$), or, equivalently, a critical amplitude of the horizontal oscillation above which the long-wave modes are unstable. The interesting result is that the number of unstable bandwidths decreases with increasing value of the viscoelastic parameter. However, in the different unstable frequency bandwidths, the dominant mode of instability intensifies with increasing value of the viscoelastic parameter. Figure 2(*b*) demonstrates the variation of $10 \times L(\beta)$ with β when $M = 0.01$ is fixed. If the surface tension is incorporated into the $O(k)$ approximation of the

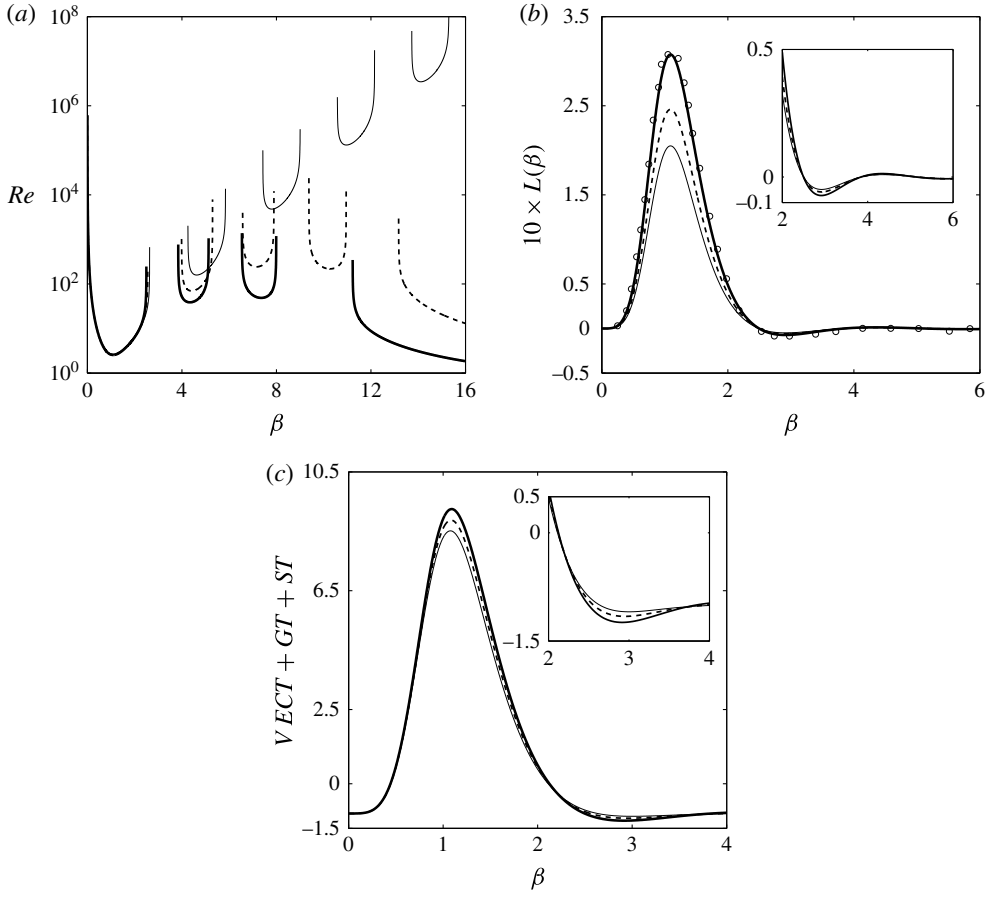

FIGURE 2. (*a*) The neutral curves in the (β, Re) plane for different values of the viscoelastic parameter when $\chi = 1$ and $\zeta^* = 0$. Here, the thick solid, dashed and thin solid lines stand for $M = 0.01$, $M = 0.005$ and $M = 0.0$ respectively. (*b*) The variation of $L(\beta)$ as a function of β when $\chi = 1$ and $M = 0.01$. Here, the thick solid, dashed and thin solid lines stand for $\zeta^* = 0$, $\zeta^* = 0.5$ and $\zeta^* = 1$ respectively. The points stand for the result of Dandapat & Gupta (1975). (*c*) The variation of $(VECT + GT + ST)$ as a function of β when $Re = 10$, $\chi = 1$ and $\zeta^* = 1$. Here, the thick solid, dashed and thin solid lines stand for $M = 0.01$, $M = 0.005$ and $M = 0$ respectively.

long-wavelength analysis, $L(\beta)$, or, equivalently, the growth rate of the long-wave mode, diminishes with increasing value of ζ^*. Therefore, one can conclude that the viscoelastic parameter has a destabilizing influence and the surface tension has a stabilizing influence on the long-wave mode in the unstable frequency bandwidths for an oscillatory viscoelastic film flow. The stabilizing effect of surface tension also supports the analytical expression given in (4.25). The variation of $10 \times L(\beta)$ with ζ^* in the higher-frequency zone ($\beta \geqslant 2$) can be found as an inset in figure 2(*b*). Further, the present result captures the result of Dandapat & Gupta (1975) very well when the surface tension parameter ζ^* is set to zero. In order to provide further evidence of the destabilizing effect of viscoelasticity on the long-wave mode, the sum $(VECT + GT + ST)$ of the different terms in the expression of the Floquet exponent (4.25) is depicted in figure 2(*c*) for different values of M when the Galileo number

χ and the modified capillary number ζ^* are fixed. Indeed, the sum is enhanced with increasing value of the viscoelastic parameter, or, equivalently, the magnitude of the viscoelastic coupling term increases with M because both GT and ST are constants. This fact results in growth of the Floquet exponent and supports the destabilizing effect of M. In other words, the destabilizing effect of the viscoelastic parameter on the long-wave mode can also be described somewhat in the spirit of Smith (1990), Huang & Khomami (2001) and Wei (2005). If an infinitesimal disturbance is considered on the unsteady base flow, a perturbation shear stress, which is a combination of the Newtonian viscous stress and the elastic stress (see (3.5)), evolves at the free surface to maintain the stress-free surface. As a result, the energy, which is greater in comparison with the Newtonian case, is transferred from the base flow to the disturbed surface through the tangential stress balance equation (3.5). In addition, this perturbation shear stress drives an unsteady advective flow under the disturbance with non-zero perturbation streamwise and cross-streamwise velocity components because the leading-order stream function is non-zero ($\phi_0 \neq 0$). The energy of this advective flow is supplied by the work done by the perturbation shear stress. The perturbation cross-streamwise velocity component pushes the fluid towards the disturbance crest through the elastic and viscous stresses, while the hydrostatic pressure and the surface tension pull the fluid away from the disturbance crest. The net force intensifies the growth of an infinitesimal disturbance, and this yields a destabilizing effect of the viscoelastic parameter.

5. Stability analysis for an arbitrary wavenumber

Numerical solution of the OS BVP (3.8)–(3.12) is carried out for disturbances of arbitrary wavenumbers. The Chebyshev spectral collocation method (Schmid & Henningson 2001) is used to recast the OS BVP into a matrix equation (Or 1997; Or & Kelly 1998),

$$2\beta^2 \mathbb{B}\partial_t \boldsymbol{\Phi} = \mathbb{A}\boldsymbol{\Phi} + (\mathbb{F}_c \cos t + \mathbb{F}_s \sin t)\boldsymbol{\Phi}, \tag{5.1}$$

where $\boldsymbol{\Phi} = [\phi_0, \phi_1, \ldots, \phi_m, \eta]^{\mathrm{T}}$ is a column matrix and $\mathbb{A}$, $\mathbb{B}$, $\mathbb{F}_c$ and $\mathbb{F}_s$ are $(m+1) \times (m+1)$ square matrices. As the Chebyshev polynomials are defined over the domain $[-1, 1]$, the liquid layer domain $y \in [-1, 0]$ is shifted to $z \in [-1, 1]$ by applying a transformation $y = (z-1)/2$. Consequently, the corresponding derivatives are replaced by $\mathcal{D} \to 2\mathcal{D}$, $\mathcal{D}^2 \to 4\mathcal{D}^2$, and so on. Next, the matrix equation (5.1) is resolved based on the Floquet theory along with the Newton–Raphson iterative scheme (Or 1997). In this method, any disturbance can be expressed in the form of a truncated complex Fourier series,

$$\boldsymbol{\Phi}(t) = \sum_{n=-k}^{n=k} \Phi_n \exp[(\mathrm{i}n + \delta)t], \tag{5.2}$$

where Φ_n represents the constant coefficient vectors and $\delta = \delta_r + \mathrm{i}\delta_i$ is the complex Floquet exponent. By substituting (5.2) into (5.1) and collecting the coefficients of Fourier components $\exp[(\mathrm{i}n + \delta)t]$, we obtain a matrix difference equation,

$$[\mathbb{A} - 2\beta^2(\delta + \mathrm{i}n)\mathbb{B}]\Phi_n = -[\mathbb{F}\Phi_{n+1} + \mathbb{F}^*\Phi_{n-1}], \tag{5.3}$$

where $\mathbb{F} = (\mathbb{F}_c + \mathrm{i}\mathbb{F}_s)/2$ and $\mathbb{F}^*$ is the complex conjugate of $\mathbb{F}$. At $n = k$, the difference equation (5.3) is reduced to the following form:

$$\Phi_k = -[\mathbb{A} - 2\beta^2(\delta + \mathrm{i}k)\mathbb{B}]^{-1}\mathbb{F}^*\Phi_{k-1} = \mathbb{R}_k\Phi_{k-1}, \tag{5.4}$$

M	β	Analytical result $(10 \times L(\beta))$	Numerical result $(10 \times L(\beta))$	Yih (1968)
0	1	2.7858	2.7869	2.7859
0.005	1	2.8793	2.8798	—
0.01	1	2.9749	2.9759	—

TABLE 1. Comparison between the long-wavelength analytical result and the numerical result for $\beta = 1$ and $\zeta^* = 0$.

where $\mathbb{R}_k = -[\mathbb{A} - 2\beta^2(\delta + \mathrm{i}k)\mathbb{B}]^{-1}\mathbb{F}^*$. By successive backward substitution, we can show

$$\Phi_n = \mathbb{R}_n \Phi_{n-1}, \quad \text{where } \mathbb{R}_n = -[\mathbb{A} - 2\beta^2(\delta + \mathrm{i}n)\mathbb{B} + \mathbb{F}\mathbb{R}_{n+1}]^{-1}\mathbb{F}^*, \quad 1 \leqslant n \leqslant (k-1). \tag{5.5}$$

At $n = -k$, the difference equation (5.3) is reduced to the following form:

$$\Phi_{-k} = -[\mathbb{A} - 2\beta^2(\delta - \mathrm{i}k)\mathbb{B}]^{-1}\mathbb{F}\Phi_{-k+1} = \mathbb{R}_{-k}\Phi_{-k+1}, \tag{5.6}$$

where $\mathbb{R}_{-k} = -[\mathbb{A} - 2\beta^2(\delta - \mathrm{i}k)\mathbb{B}]^{-1}\mathbb{F}$. Similarly, by successive forward substitution, we can show

$$\Phi_{-n} = \mathbb{R}_{-n}\Phi_{-n+1}, \quad \text{where } \mathbb{R}_{-n} = -[\mathbb{A} - 2\beta^2(\delta - \mathrm{i}n)\mathbb{B} + \mathbb{F}^*\mathbb{R}_{-(n+1)}]^{-1}\mathbb{F}, \quad 1 \leqslant n \leqslant k-1. \tag{5.7}$$

Using (5.5) and (5.7), at $n = 0$, (5.3) can be recast into a homogeneous algebraic system,

$$[\mathbb{A} - 2\beta^2\delta\mathbb{B} + \mathbb{F}\mathbb{R}_1 + \mathbb{F}^*\mathbb{R}_{-1}]\Phi_0 = 0. \tag{5.8}$$

Hence, for a non-trivial solution of Φ_0, the determinant must vanish, which implies

$$\det[\mathbb{A} - 2\beta^2\delta\mathbb{B} + \mathbb{F}\mathbb{R}_1 + \mathbb{F}^*\mathbb{R}_{-1}] = 0. \tag{5.9}$$

Here, we shall focus solely on the synchronous solutions ($\delta_i = 0$). In particular, the matrix equation (5.1) belongs to a class of equations that cannot describe the subharmonic solutions (Or 1997).

All of the numerical computations are performed for 21 Chebyshev modes ($m = 21$) and 28 Fourier modes ($k = 14$), which is sufficient to achieve accurate numerical results. Further, if the number of Chebyshev modes is increased by 2, the results change by less than 0.1 % only in the higher-frequency regime ($\beta > 6$). The validation of the numerical result and the long-wavelength analytical result can be found in table 1. In order to explore the finite wavenumber results and to compare with those for a Newtonian liquid (Or 1997), the numerical test is carried out for two different values of the viscoelastic parameter M when $\chi = 1$ and $\zeta = 0.05$ are fixed. Here, we choose $M = 0$ and $M = 0.005$. The results are illustrated in figure 3. Unlike the long-wave analytical result, the U-shaped neutral curves appear in different frequency ranges at $k \to 0$. If the wavenumber is increased gradually, branch points are detected on the U-shaped neutral curves. This fact indicates that one branch may continue with the Reynolds number at long wavelength ($k \to 0$), while another branch may continue with the frequency at finite wavenumber. Indeed, the new finite-k neutral curves, indicated by an oblique thick line ($M = 0.005$) and an oblique thin line ($M = 0$), emerge from the branch points and grow monotonically with β until the curves intersect the next U-shaped neutral curve. In fact, these new finite-k oblique

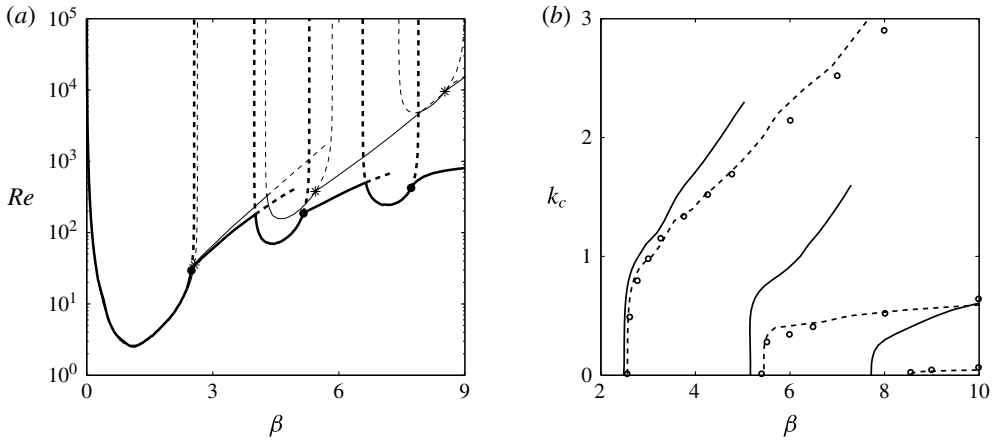

FIGURE 3. (*a*) The neutral curve in the (β, *Re*) plane when $\chi = 1$ and $\zeta = 0.05$. Here, the thick and thin lines stand for $M = 0.005$ and $M = 0$ respectively. The branch points are indicated by solid circles ($M = 0.005$) and stars ($M = 0$). (*b*) The variation of the critical wavenumber as a function of β. Here, the solid and dashed lines stand for $M = 0.005$ and $M = 0$ respectively. The points stand for the result of Or (1997).

neutral curves are no longer confined to the regime of long-wave unstable frequency bandwidths. Instead, these curves lie in the regime of long-wave stable frequency bandwidths. Consequently, the long-wave stabilizing effect of viscoelasticity in these stable frequency bandwidths is no longer valid when the wavenumber is finite. In particular, in these stable frequency bandwidths, the instability is dominated by the finite wavenumber modes. In addition, in the long-wave frequency bandwidths, the most unstable mode is intensified in the presence of the viscoelastic parameter, which fully agrees with the analytical result discussed in § 4. Obviously, the viscoelastic parameter has a significant impact on the instability in the higher-frequency zone $\beta > 3$; i.e. the presence of viscoelasticity makes the intensities of the long-wave and finite wavenumber modes stronger. The separation distance between branch points corresponding to Newtonian liquid and non-Newtonian liquid grows successively with increasing value of M. Moreover, the finite-k oblique neutral curves emerging from the branch points have finite critical wavenumbers k_c, which alter with the dimensionless oscillation frequency β (see figure 3*b*). It should be noted that the viscoelastic parameter has a significant influence also on the finite critical wavenumbers k_c. It is observed that the critical wavenumbers corresponding to all of the branches of the finite-k neutral curves grow monotonically with β, and this fact is in contrast to the result for Newtonian liquid (Or 1997), where the critical wavenumbers k_c associated with the higher branches of the finite-k neutral boundaries approach a constant value asymptotically at sufficiently large frequency β.

Now, the neutral curves are analysed thoroughly in the local neighbourhood of the branch points. The first branch point is detected at $\beta = 2.4925$, which is different from the value of $\beta = 2.563$ obtained for a Newtonian liquid (Or 1997). Figure 4(*a*) shows the neutral curves in the (k, *Re*) plane for two different values of β. The lower solid neutral curve shows a monotonic shape at a slightly lower value, $\beta = 2.4922$, than the branch point. Therefore, this neutral curve has a single minimum at $k \to 0$, which signals that the long-wave mode is more unstable than the finite wavenumber mode. On the contrary, the upper solid neutral curve has a non-monotonic shape

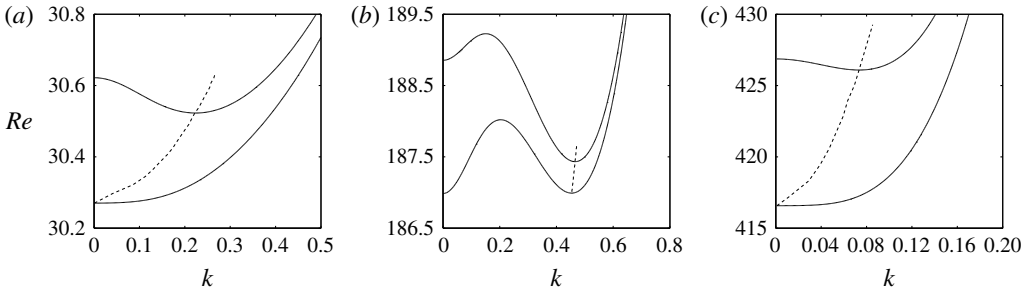

FIGURE 4. (*a*) The neutral curves in the local neighbourhood of the first branch point when $\chi = 1$, $M = 0.005$ and $\zeta = 0.05$. (*b*) The neutral curves in the local neighbourhood of the second branch point. (*c*) The neutral curves in the local neighbourhood of the third branch point.

at a slightly higher value, $\beta = 2.4935$, than the branch point. The local minimum is detected at $k = 0.22$, which signals that the finite wavenumber mode is more dangerous than the long-wave mode. Obviously, the long-wave instability switches to the finite wavenumber instability exactly at the branch point. In fact, this switching process proceeds in a continuous fashion, which is illustrated by a dash-dotted line in figure 4(*a*). The variation of the neutral curves in the local neighbourhood of the second branch point, $\beta = 5.1590$, is shown in figure 4(*b*). It should be noted that both curves show a non-monotonic shape, which is in contrast to the previous result. When $\beta = 5.1586$, the neutral curve has a local minimum at $k \to 0$, which indicates the dominant effect of the long-wave mode. On the other hand, the local minimum shifts to $k = 0.46$ at $\beta = 5.1610$, which indicates the dominant effect of the finite wavenumber mode. Again, the long-wave instability switches to the finite wavenumber instability through the second branch point, but in a discontinuous fashion. It seems that a competition occurs between the long-wave mode and the finite wavenumber mode in the vicinity of the branch points. Figure 4(*c*) illustrates the resulting neutral curves in the local neighbourhood of the third branch point at $\beta = 7.72$. In this case, the lower solid neutral curve shows a monotonic shape at a slightly lower value, $\beta = 7.7165$, than the branch point. Therefore, this neutral curve has a single minimum at $k \to 0$, which signals that the long-wave mode is more unstable than the finite wavenumber mode. On the contrary, the upper solid neutral curve has a non-monotonic shape at a slightly higher value, $\beta = 7.725$, than the branch point. The local minimum appears at $k = 0.073$, which is a small value in comparison with the previous two cases. However, the dash-dotted curve representing the stability limit grows monotonically with wavenumber k. Therefore, in this case also, the long-wave instability switches to the finite wavenumber instability through the third branch point. However, this switching process proceeds in a continuous fashion as in the first case.

Now, the numerical test is performed for a comparatively large value of the viscoelastic parameter, $M = 0.01$, as proposed by Dandapat & Gupta (1975). The associated results are depicted in figure 5(*a*). Here, we shall focus only on the third U-shaped neutral curve because the finite wavenumber neutral curve emerging from the branch point of the third U-shaped neutral curve is no longer an oblique line. Therefore, the finite wavenumber neutral curve requires thorough investigation close to the third branch point in the (k, Re) plane. To do this, the numerical test is performed with $\beta = 7.94$, a value on the long-wave neutral curve. Figure 5(*b*)

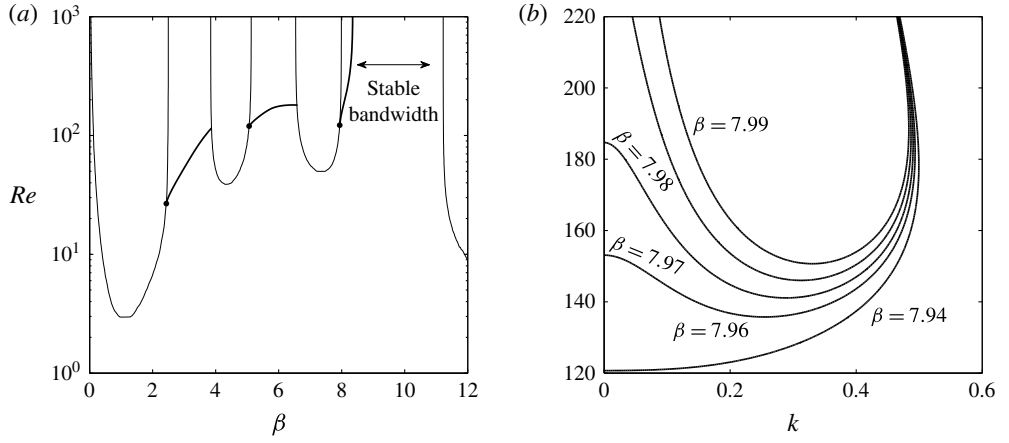

FIGURE 5. (*a*) The neutral curves in the (β, *Re*) plane when $M = 0.01$, $\chi = 1$ and $\zeta = 0.05$. Here, the thick and thin lines represent the results corresponding to the long-wavelength and finite wavelength analyses. The branch points are indicated by solid circles. (*b*) The scenario of neutral curves in the (k, *Re*) plane for different values of β.

shows the associated neutral curve whose local minimum appears at $k \to 0$, and this fact indicates the dominant effect of the long-wave mode on the instability. If β continues to increase gradually along the finite wavenumber neutral curve through the branch point, the local minimum shifts to the finite wavenumber region, and this fact indicates the dominant effect of the finite wavenumber mode on the instability. Again, the long-wave instability switches to the finite wavenumber instability. The associated neutral curves exhibit a tongue-like shape. In this case, there exists a stable bandwidth because the finite wavenumber neutral curve emerging from the branch point of the third U-shaped long-wave neutral curve never intersects the next U-shaped long-wave neutral curve.

6. Conclusions

A linear stability analysis of a viscoelastic liquid film on an oscillating plane is carried out for disturbances of arbitrary wavenumbers. The Orr–Sommerfeld equation is derived for an unsteady base flow. In the long-wave regime, the analytical solution of the time-dependent Orr–Sommerfeld equation is supplied by using the Floquet theory along with the normal mode decomposition. It is noticed that the long-wave modes can grow only in the separated unstable bandwidths of the imposed frequency. In these unstable frequency bandwidths, the most unstable mode becomes stronger in the presence of the viscoelastic parameter. Outside these unstable frequency bandwidths, all infinitesimal disturbances will decay, i.e. the long-wavelength analysis predicts some stable bandwidths of the imposed frequency. Further, in each unstable frequency bandwidth, the long-wave modes are unstable only if the associated Reynolds number exceeds a critical value, or, equivalently, if the amplitude of the horizontal oscillation exceeds a critical value. In addition, the long-wave unstable mode is attenuated in the presence of surface tension.

The Chebyshev spectral collocation method is used to resolve the OS BVP for disturbances of arbitrary wavenumbers. It is observed that branch points appear on the long-wave neutral curves when the wavenumber continues to increase. The finite

wavenumber neutral curves emerging from the branch points of the long-wave neutral curves are no longer confined to the separated unstable bandwidths of the imposed frequency. Instead, these curves extend into the entire regime of the long-wave stable bandwidths of the imposed frequency. Therefore, there does not exist any stable frequency bandwidth in the finite wavenumber regime where the viscoelastic parameter shows a stabilizing effect. This fact is in contrast to the result in the long-wave regime, where instability occurs only in the separated unstable bandwidths of the imposed frequency. However, at $M = 0.01$, a stable frequency bandwidth is still found in the large-frequency regime when the wavenumber is finite. Moreover, it is shown that the long-wave instability switches to the finite wavenumber instability through the branch points in either a continuous or a discontinuous fashion. Therefore, one can conclude that the finite wavenumber instability is more dangerous than the long-wave instability in some frequency ranges.

Acknowledgement

I would like to thank the anonymous referees for their comments and constructive suggestions to improve this paper.

REFERENCES

ANDERSSON, H. I. & DAHL, E. N. 1999 Gravity-driven flow of a viscoelastic liquid film along a vertical wall. *J. Phys. D: Appl. Phys.* **32**, 1557–1562.

BARNES, H. A., HUTTON, J. F. & WALTERS, K. 1989 *An Introduction to Rheology*. Elsevier.

BEARD, D. W. & WALTERS, K. 1964 Elastico-viscous boundary-layer flows I. Two-dimensional flow near a stagnation point. *Proc. Camb. Phil. Soc.* **60**, 667–674.

BIRD, R. B., CURTISS, C. F., ARMSTRONG, R. C. & HASSAGER, O. 1987 *Dynamics of Polymer Liquids*, vols. 1 and 2. Wiley.

BURYA, A. G. & SHKADOV, V. YA. 2001 Stability of a liquid film flowing down an oscillating inclined surface. *Fluid Dyn.* **36**, 671–681.

DANDAPAT, B. S. & GUPTA, A. S. 1975 Instability of a horizontal layer of viscoelastic liquid on an oscillating plane. *J. Fluid Mech.* **72**, 425–432.

DÁVALOS-OROZCO, L. A. 2013 Stability of thin viscoelastic flims down wavy walls. *Interfacial Phenomena Heat Transfer* **1**, 301–315.

GAO, P. & LU, X.-Y. 2006 Effect of surfactants on the long-wave stability of oscillatory film flow. *J. Fluid Mech.* **562**, 345–354.

GAO, P. & LU, X.-Y. 2008 Instability of an oscillatory fluid layer with insoluble surfactants. *J. Fluid Mech.* **595**, 461–490.

GROTBERG, J. B. & JENSEN, O. E. 2004 Biofluid mechanics in flexible tubes. *Annu. Rev. Fluid Mech.* **36**, 121–147.

HUANG, C.-T. & KHOMAMI, B. 2001 The instability mechanism of single and multi-layer Newtonian and viscoelastic flows down an inclined plane. *Rheol. Acta* **40**, 467–484.

IKBAL, MD. A. 2012 Viscoelastic blood flow through arterial stenosis – effect of variable viscosity. *Intl J. Non-Linear Mech.* **47**, 888–894.

LARSON, R. G. 1992 Instabilities in viscoelastic flows. *Rheol. Acta* **31**, 213–263.

LIN, S. P., CHEN, J. N. & WOODS, D. R. 1996 Suppression of instability in a liquid film flow. *Phys. Fluids* **8**, 3247–3252.

OLDROYD, J. G. 1950 On the formulation of rhelogical equations of state. *Proc. R. Soc. Lond.* A **200**, 523–541.

OR, A. C. 1997 Finite-wavelegth instability in a horizontal liquid layer on an oscillating plane. *J. Fluid Mech.* **335**, 213–232.

OR, A. C. & KELLY, R. E. 1998 Thermocapillary and oscillatory-shear instabilities in a layer of liquid with a deformable surface. *J. Fluid Mech.* **360**, 21–39.

SAMANTA, A. 2009 Effect of electric field on the stability of an oscillatory contaminated film flow. *Phys. Fluids* **21**, 114101.

SAVINS, J. G. 1967 A stress-controlled drag-reduction phenomenon. *Rheol. Acta* **6**, 323–330.

SCHMID, P. & HENNINGSON, D. 2001 *Stability and Transition in Shear Flows*. Springer.

SHAQFEH, E. S. G. 1996 Purely elastic instabilities in viscometric flows. *Annu. Rev. Fluid Mech.* **28**, 129–185.

SMITH, M. K. 1990 The mechanism for the long-wave instability in thin liquid films. *J. Fluid Mech.* **217**, 469–485.

WALTERS, K. 1960 The motion of an elastico-viscous liquid contained between coaxial cylinders (II). *Q. J. Mech. Appl. Maths* **13**, 444–461.

WEI, H. H. 2005 Stability of a viscoelastic falling film with surfactant subject to an interfacial shear. *Phys. Rep.* **71**, 066306.

WOODS, D. R. & LIN, S. P. 1995 Instability of a liquid film flow over a vibrating inclined plane. *J. Fluid Mech.* **294**, 391–407.

YIH, C. S. 1968 Instability of unsteady flows or configurations. Part 1. Instability of a horizontal liquid layer on an oscillating plane. *J. Fluid Mech.* **31**, 737–751.